Finite Element P1 Solution of Thermal Flow past a Circular Cylinder with Radiation (SI - CMMSE - 2006)

Mohammed Seaid, El-Amrani Mofdi

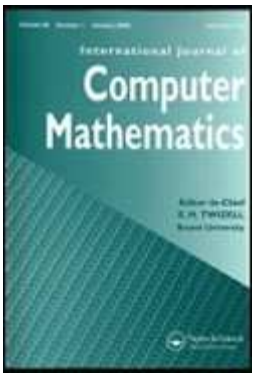

Finite Element P1 Solution of Thermal Flow past a Circular Cylinder with Radiation (SI - CMMSE - 2006)

Journal:	*International Journal of Computer Mathematics*
Manuscript ID:	GCOM-2006-0156.R1
Manuscript Type:	Original Article
Date Submitted by the Author:	27-Nov-2006
Complete List of Authors:	Seaid, Mohammed; Universität Kaiserslautern, Fachbereich Mathematik, AG Technomathematik Mofdi, El-Amrani; Universidad Rey Juan Carlos, Departamento de Matemática Aplicada
Keywords:	Radiative transfer, Finite element method, Simplified P1 model, Flow past a cylinder, Galerkin-characteristic scheme

International Journal of Computer Mathematics
Vol. 00, No. 00, Month 200x, 1–16

Finite Element $\mathbf{P_1}$ *Solution of Unsteady Thermal Flow past a Circular Cylinder with Radiation* (SI - CMMSE - 2006)

Mohammed Seaïd*† and Mofdi El-Amrani‡

†Fachbereich Mathematik, Technische Universität Kaiserslautern, D-67663 Kaiserslautern, Germany
‡Dpto. Matemática Aplicada, Universidad Rey Juan Carlos, c/Tulipán s/n, 28933 Móstoles-Madrid, Spain

(*v3.2 released May 2006*)

We propose a finite element method for solving combined convection and radiation in laminar flow past a circular cylinder. The flow problem is described by the thermal incompressible Navier-Stokes equations subject to a Boussinesq approach. To incorporate radiation into the model we consider a simplified P_1 approximation of the radiative transfer equation. The numerical solution of the governing equations is performed by a Galerkin-characteristic method using finite element discretization. The method is accurate and stable for a wide range of optical scales and Reynolds numbers. In addition, the characteristic treatment in the method eliminates most of the numerical difficulties appear usually in the Eulerian-based methods for convection-dominated problems. Numerical results are presented and comparisons between simulations with and without radiation are also illustrated.

Keywords: Radiative transfer; Finite element method; Simplified P_1 model; Flow past a cylinder; Galerkin-characteristic scheme

AMS Subject Classifications: 85A25; 76M10; 76D05

1. Introduction

Numerical study of flow past a cylinder is of practical importance in engineering applications. In many engineering designs, circular cylinders constitute the basic component of structures, for example, heat exchange tubes, cooling systems for nuclear power plants, offshore structures, cooling towers, chimney stacks and transmission cables, etc. The fluid flow in those structures can be gas, water or malted glass, among others. In many interesting situations, experimental and numerical simulations help to enrich the knowledge concerned. The isothermal incompressible flow past a cylinder has been well studied and considered as a benchmark problem for validating new numerical techniques in computational fluid dynamics (CFD), compare [5, 10, 20, 28] and further references are therein. Recently, the thermal version of this problem has been investigated in [6,13]. In the above mentioned references no radiation effects have been incorporated in the system. However, growing concern with high temperature processes has emphasized the need for an evaluation of the effect of radiative heat transfer. Nevertheless, it is common for work on convective flows to neglect thermal radiation mainly because it involves tedious mathematics, which increase the computational work, and also because of the lack of detailed information on optical properties of the participating media and surfaces. However, radiation can strongly interact with convection in many situations of engineering interest and neglecting its effects may have significant consequences in the overall predictions. The aim of the present work is to demonstrate the effect of radiation in producing benchmark results, in this case for laminar flow past a circular cylinder, as now illustrated.

In this paper, we provide our numerical solutions for radiation-convection flow past a circular cylinder. The radiation effects are included into the thermal incompressible Navier-Stokes equations through a simplified P_1 (SP_1) problem. The SP_1 model is obtained using an asymptotic analysis in the radiative transfer

*Corresponding author. Email: seaid@mathematik.uni-kl.de

International Journal of Computer Mathematics
ISSN 0020-7160 print/ISSN 1029-0265 online
http://www.tandf.co.uk/journals
DOI: 10.1080/0020716YYxxxxxxxx

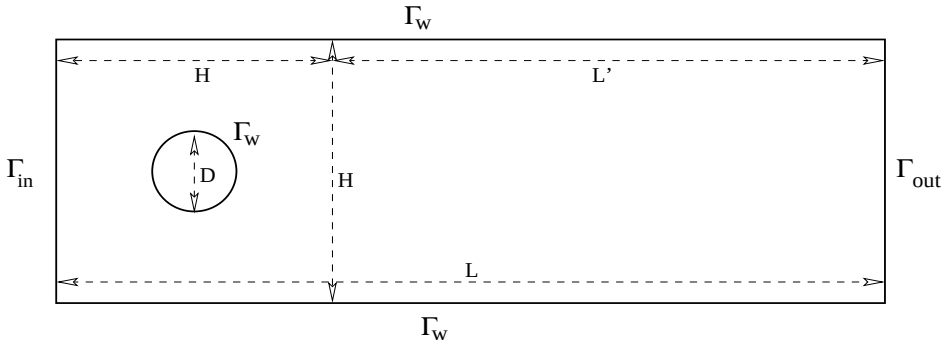

Figure 1. Geometry of the flow past a cylinder.

equation, we refer the reader to [16] for details on the derivation of generalized simplified P_N approximations. The SP_1 model has proved its capability to provide efficient and yet accurate approximation of radiative heat transfer problems in optically thick media. To the best of our knowledge, this paper is the first to report numerical results for coupled radiation-convection flow over a circular cylinder. The results of the present study are useful for providing comparative data and developing accurate and robust solvers for radiative heat transfer and fluid flow computations.

To numerically solve the governing equations we develop a characteristic-based method in finite elements framework. In Galerkin-characteristic methods, the time derivative and the advection term are combined as a directional derivative along the characteristics, leading to a characteristic time-stepping procedure. Consequently, the Galerkin-characteristic methods symmetrize and stabilize the governing equations, allow for large time steps in a simulation without loss of accuracy, and eliminate the excessive numerical dispersion and grid orientation effects present in many upwind methods, compare for example [3, 6, 14]. A Galerkin-characteristic algorithm has been successfully applied to isothermal incompressible Navier-Stokes equations in [5]. Application of this method to thermal viscous incompressible flows has recently been investigated by the authors in [6]. The current work presents an extension of the method to combined radiation and convection flows.

This paper is organized as follows. The governing equations for coupled radiation and convection are presented in section 2. In section 3 we introduce the simplified P_1 approximation of the radiative transfer equation. The solution procedure and the numerical methods are formulated in section 4. Section 5 contains the numerical results showing the performance of the proposed methods. Some concluding remarks complete the study in section 6.

2. Equations for Radiation-Convection Flows

A schematic of the system considered in the present work is shown in Figure 1. The system consists of a viscous thermal radiating flow in a channel containing a circular cylinder. The isothermal version of this example has been subject of many numerical validations for laminar flows, see for instance [10,20,28]. Here, the channel width is L, the channel height is H and the diameter of cylinder is D. A viscous incompressible fluid flow at cold temperature T'_C enters through the left boundary of channel with uniform velocity u_∞ while, the upper and lower walls are kept at hot temperature T'_H. The cylinder wall is also kept at the hot temperature T'_H. The fluid is Newtonian and all the thermophysical properties are assumed to be constant, except for density in the buoyancy term that can be adequately modelled by the Boussinesq approximation [11] and that compression effects and viscous dissipation are neglected. With these assumptions, the governing equations are

Conservation of mass:

$$\frac{\partial u'}{\partial x} + \frac{\partial v'}{\partial y} = 0. \tag{1}$$

Conservation of momentum:

$$\frac{\partial u'}{\partial t} + u'\frac{\partial u'}{\partial x} + v'\frac{\partial u'}{\partial y} + \frac{1}{\rho}\frac{\partial p'}{\partial x} = \mu\left(\frac{\partial^2 u'}{\partial x^2} + \frac{\partial^2 u'}{\partial y^2}\right), \tag{2}$$

$$\frac{\partial v'}{\partial t} + u'\frac{\partial v'}{\partial x} + v'\frac{\partial v'}{\partial y} + \frac{1}{\rho}\frac{\partial p'}{\partial y} = \mu\left(\frac{\partial^2 v'}{\partial x^2} + \frac{\partial^2 v'}{\partial y^2}\right) + g'\beta'\left(T' - T_\infty\right). \tag{3}$$

Conservation of energy:

$$\rho_\infty c_p\left(\frac{\partial T'}{\partial t} + u'\frac{\partial T'}{\partial x} + v'\frac{\partial T'}{\partial y}\right) = \lambda\left(\frac{\partial^2 T'}{\partial x^2} + \frac{\partial^2 T'}{\partial y^2}\right) - \nabla\cdot q'_R, \tag{4}$$

where T_∞ is the reference temperature, ρ_∞ the reference density, $\mathbf{u}' = (u', v')^T$ the velocity field, p' the pressure, T' the temperature, μ the dynamic viscosity, c_p the specific heat at constant pressure, g' the gravity force, β' the coefficient of thermal expansion, and λ the thermal diffusivity coefficient. We used primed variables to denote dimensional quantities. The effect of radiation is taken into consideration in the energy equation as the divergence of radiative heat flux, q'_R. For a grey medium, this term is given by

$$-\nabla\cdot q'_R = \int_{\mathbb{S}^2} \kappa\Big(B'(T') - I'\Big)\, d\omega, \tag{5}$$

where $\mathbb{S}^2$ denotes the unit sphere and $I'(\omega, \mathbf{x})$ is the spectral intensity at position $\mathbf{x}$ and propagating along direction ω. For a non-scattering medium, the intensity I' is obtained from the radiative transfer equation

$$\omega\cdot\nabla I' + \kappa I' = \kappa B'(T'), \tag{6}$$

where κ is the absorption coefficient and $B'(T)$ is the spectral intensity of the black-body radiation given by the Planck function

$$B'(T) = \sigma_B T'^4, \tag{7}$$

with σ_B is the Boltzmann constant. For more details on the equations of radiation hydrodynamics we refer to [17, 18] among others. Since it is convenient to work with dimensionless formulations, we define the following nondimensional variables

$$\mathbf{x} = \frac{\mathbf{x}'}{D}, \qquad t = \frac{u_\infty t'}{D}, \qquad \mathbf{u} = \frac{\mathbf{u}'}{u_\infty}, \qquad p = \frac{p' - \rho_\infty}{\rho_\infty u_\infty^2}, \qquad I = \frac{I}{I_\infty},$$
$$\mathbf{g} = \frac{D\mathbf{g}'}{u_\infty^2}, \qquad T = \frac{T' - T_C}{T_H - T_C}, \qquad \beta = \beta'(T_H - T_C), \qquad T_0 = \frac{T_\infty}{T_H - T_C},$$

with the subscript '∞' presents the reference quantities. We also define the optical scale τ, the Prandtl number Pr, the Reynolds number Re, and the Planck number Pl, as

$$\tau = \frac{1}{\kappa_{\text{ref}} D}, \qquad Pr = \frac{\mu}{\rho_\infty \lambda}, \qquad Re = \frac{\rho_\infty D u_\infty}{\mu}, \qquad Pl = \frac{\lambda\,(T_H - T_C)}{D\sigma_B T_C^4}. \tag{8}$$

Hence, the equations (1)-(4) can be rewritten in dimensionless form as

$$\begin{aligned} \nabla \cdot \mathbf{u} &= 0, \\ \frac{D\mathbf{u}}{Dt} + \nabla p - \frac{1}{Re}\nabla^2 \mathbf{u} &= \left(T - \frac{1}{2}\right)\mathbf{e}, \\ \frac{DT}{Dt} - \frac{1}{PrRe}\nabla^2 T &= -\frac{1}{PrRe}\nabla \cdot q_R, \end{aligned} \tag{9}$$

where $\mathbf{e} = (0,1)^T$ is the unit vector in direction of the gravitational force and the material derivative $\frac{Dw}{Dt}$ of a generic function w is defined as

$$\frac{Dw}{Dt} = \frac{\partial w}{\partial t} + \mathbf{u} \cdot \nabla w. \tag{10}$$

The dimensionless radiative heat term is given by

$$-\nabla \cdot q_R = \frac{1}{\tau Pl}\big(B(T) - \varphi\big), \tag{11}$$

where φ is the radiative energy defined as

$$\varphi(\mathbf{x}) = \int_{\mathbb{S}^2} I(\omega, \mathbf{x})\, d\omega. \tag{12}$$

The dimensionless function B is given by

$$B(T) = 4\left(\frac{T}{T_0} + 1\right)^4.$$

The radiative transfer equation (6) can be rewritten in dimensionless form as

$$\tau\omega \cdot \nabla I + \kappa I = \kappa B(T). \tag{13}$$

The governing equations (9) and (13) are solved on a computational domain Ω with smooth boundary $\partial\Omega = \Gamma_{\rm w} \cup \Gamma_{\rm in} \cup \Gamma_{\rm out}$, as shown in Figure 1, and subject to the following boundary conditions

$$\begin{aligned} \mathbf{u}(t, \hat{\mathbf{x}}) &= \mathbf{0}, && \forall\, \hat{\mathbf{x}} \in \Gamma_{\rm w}, \\ u(t, \hat{\mathbf{x}}) &= u_\infty, && \forall\, \hat{\mathbf{x}} \in \Gamma_{\rm in}, \\ -p\mathbf{n}(\hat{\mathbf{x}}) + \frac{1}{Re}\mathbf{n}(\hat{\mathbf{x}}) \cdot \nabla \mathbf{u}(t, \hat{\mathbf{x}}) &= \mathbf{0}, && \forall\, \hat{\mathbf{x}} \in \Gamma_{\rm out}, \end{aligned} \tag{14}$$

for the flow, and

$$\begin{aligned} T(t, \hat{\mathbf{x}}) &= T_H, && \forall\, \hat{\mathbf{x}} \in \Gamma_{\rm w}, \\ T(t, \hat{\mathbf{x}}) &= T_C, && \forall\, \hat{\mathbf{x}} \in \Gamma_{\rm in}, \\ \mathbf{n}(\hat{\mathbf{x}}) \cdot \nabla T(t, \hat{\mathbf{x}}) &= 0, && \forall\, \hat{\mathbf{x}} \in \Gamma_{\rm out}, \end{aligned} \tag{15}$$

for the temperature. Here, $\mathbf{n}(\hat{\mathbf{x}})$ denotes the outward unit normal in $\hat{\mathbf{x}}$ with respect to $\partial\Omega$. For the radiative

transfer, the boundary conditions are for diffuse emitting and reflecting walls

$$\begin{aligned} I(\hat{\mathbf{x}},\omega) &= B(T_H), && \forall\, \hat{\mathbf{x}} \in \Gamma^-_{\mathrm{w}}, \\ I(\hat{\mathbf{x}},\omega) &= B(T_C), && \forall\, \hat{\mathbf{x}} \in \Gamma^-_{\mathrm{in}}, \\ I(\hat{\mathbf{x}},\omega) &= I(\hat{\mathbf{x}},\omega'), && \forall\, \hat{\mathbf{x}} \in \Gamma^-_{\mathrm{out}}, \end{aligned} \tag{16}$$

where ω' is the specular reflection of ω on the surface Γ_{out} and the boundary regions Γ_i^-, $i \in \{\mathrm{w}, \mathrm{in}, \mathrm{out}\}$, are defined as

$$\Gamma_i^- = \{\hat{\mathbf{x}} \in \Gamma_i : \quad \mathbf{n}(\hat{\mathbf{x}}) \cdot \omega < 0\}\,.$$

It should be stressed that nongrey media and scattering fluids can also be incorporated in our formulation without major conceptual modifications.

3. The Simplified $\mathbf{P_1}$ Approximation

A class of simplified $\mathrm{P_N}$ approximations for radiative heat transfer problems have been analyzed in [16]. The simplified $\mathrm{P_N}$ approximations have also been studied in [14, 22, 31] for glass manufacturing, in [2] for crystal growth, in [8, 23, 24] for gas turbines, and in [29] for low Mach number flows. Recently, validation of the simplified $\mathrm{P_N}$ approximations with experimental measurements has been carried out in [27] for a three-dimensional diffusion flame. In the current work, we extend the SP_1 approximations to the radiation-convection flow past a cylinder.

The starting point for deriving simplified $\mathrm{P_N}$ approximations for the radiative heat transfer is to rewrite the equation (13) as

$$\left(1 + \frac{\tau}{\kappa}\omega \cdot \nabla\right) I = B(T).$$

Then, apply a Neumann series to formally invert the transport operator

$$\begin{aligned} I &= \left(1 + \frac{\tau}{\kappa}\omega \cdot \nabla\right)^{-1} B, \\ &\approx \left(1 - \frac{\tau}{\kappa}\omega \cdot \nabla + \frac{\tau^2}{\kappa^2}(\omega \cdot \nabla)^2 + \cdots\right) B. \end{aligned}$$

Integrating respect to ω over all directions in the unit sphere $\mathbb{S}^2$ and using the relation

$$\int_{\mathbb{S}^2} (\omega \cdot \nabla)^n d\omega = \left(1 + (-1)^n\right) \frac{2\pi}{n+1} \nabla^n, \qquad \forall\, n \geq 1,$$

we obtain the formal asymptotic equation for φ

$$4\pi B = \left(1 - \frac{\tau^2}{3\kappa^2}\nabla^2 - \frac{4\tau^4}{45\kappa^4}\nabla^4\right)\varphi + \mathcal{O}(\tau^6).$$

When terms of $\mathcal{O}(\tau^2)$ or $\mathcal{O}(\tau^4)$ are neglected we obtain the simplified P_0 or simplified P_1 approximation, respectively. Higher order approximations can be derived in a similar manner, compare [16] for more details. The simplified P_0 approximation leads

$$\varphi = 4\pi B(T). \tag{17}$$

Note that the equilibrium (17) cancels the radiation effects in the energy equation (9). In this paper, we consider only the simplified P_1 approach and our techniques can be straightforwardly extended to other higher order SP_N approximations. Thus, the simplified P_1 approximation gives

$$4\pi B = \varphi - \frac{\tau^2}{3\kappa^2}\nabla^2\varphi + \mathcal{O}(\tau^4),$$

and its associated equation is given by

$$-\frac{\tau^2}{3\kappa}\nabla^2\varphi + \kappa\varphi = 4\pi\kappa B(T). \tag{18}$$

Once the radiative energy φ is obtained from the equation (18) the total radiative heat flux is formulated as in (11). The boundary conditions for the simplified P_N approximations are derived from variational principles using Marshak conditions [9, 15]. Here, we formulate boundary conditions for the SP_1 approximation which are consistent with temperature boundary conditions (15). For more general formulation of these boundary conditions we refer the reader to [16]. Hence, the boundary conditions for the SP_1 equation (18) are

$$\begin{aligned}
\frac{\tau}{3\kappa}\mathbf{n}(\hat{\mathbf{x}})\cdot\nabla\varphi(\hat{\mathbf{x}}) + \varphi(\hat{\mathbf{x}}) &= 4\pi B\left(T_H\right), && \forall\, \hat{\mathbf{x}} \in \Gamma_{\mathrm{w}},\\
\frac{\tau}{3\kappa}\mathbf{n}(\hat{\mathbf{x}})\cdot\nabla\varphi(\hat{\mathbf{x}}) + \varphi(\hat{\mathbf{x}}) &= 4\pi B\left(T_C\right), && \forall\, \hat{\mathbf{x}} \in \Gamma_{\mathrm{in}},\\
\mathbf{n}(\hat{\mathbf{x}})\cdot\nabla\varphi(\hat{\mathbf{x}}) &= 0, && \forall\, \hat{\mathbf{x}} \in \Gamma_{\mathrm{out}}.
\end{aligned} \tag{19}$$

It should be stressed that the SP_1 model is a promising approach of combining convection and radiation in participating media. The main advantage of the SP_1 equations, apart from the obvious ease with which the models can be incorporated into CFD calculations due to their compatibility with the solutions of differential equations for convective and radiating flows, they are computationally efficient and relatively easy to implement in an existing CFD software.

4. Solution Procedure

The numerical method we propose for approximating solutions to the fluid dynamics and radiation equations presented in the previous section can be interpreted as a fractional step technique where the radiation-convection part is decoupled from the Stokes/Boussinesq part in the temporal discretization. Thus, at each time step the radiative energy, velocity, temperature and pressure are updated by solving first the SP_1 equation

$$-\frac{\tau^2}{3\kappa}\nabla^2\varphi + \kappa\varphi = 4\pi\kappa B(T), \tag{20}$$

subject to boundary conditions (19). Second, the convection equations

$$\begin{aligned}
\frac{\partial \mathbf{u}}{\partial t} + \mathbf{u}\cdot\nabla\mathbf{u} &= \mathbf{0},\\
\frac{\partial T}{\partial t} + \mathbf{u}\cdot\nabla T &= 0.
\end{aligned} \tag{21}$$

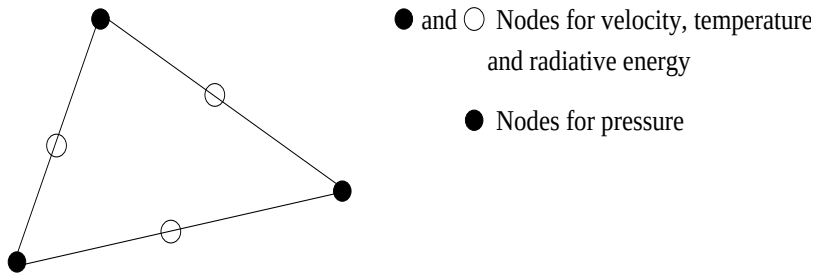

Figure 2. Taylor-Hood finite element.

Then, the Stokes/Boussinesq equations

$$\begin{aligned} \nabla \cdot \mathbf{u} &= 0, \\ \frac{\partial \mathbf{u}}{\partial t} + \nabla p - \frac{1}{Re}\nabla^2 \mathbf{u} &= \left(T - \frac{1}{2}\right)\mathbf{e}, \\ \frac{\partial T}{\partial t} - \frac{1}{PrRe}\nabla^2 T &= -\frac{1}{PrRe}\nabla \cdot q_R. \end{aligned} \tag{22}$$

supplied with boundary conditions (14) and (15). Remark that the energy equation in (22) has been decoupled from the momentum equation, which can be solved separately once the convective step (21) is approximated.

For the spatial discretization we consider the finite element method. Let h be a spatial discretization parameter such that $0 < h < h_0$ with $0 < h_0 < 1$. We generate a quasi-uniform partition $\Omega_h \subset \bar{\Omega} = \Omega \cup \partial\Omega$ of small triangles $\mathcal{T}_j$ that satisfy the following conditions:

(i) $\bar{\Omega} = \bigcup_{j=1}^{Ne} \mathcal{T}_j$, where Ne is the number of triangles of Ω_h.

(ii) If $\mathcal{T}_i$ and $\mathcal{T}_j$ are two different triangles of Ω_h, then

$$\mathcal{T}_i \cap \mathcal{T}_j = \begin{cases} P_{ij}, & \text{a mesh point, or} \\ \Gamma_{ij}, & \text{a common side, or} \\ \emptyset, & \text{empty set.} \end{cases}$$

(iii) There exists a positive constant k such that for all $j \in \{1, \cdots, Ne\}$, $\frac{d_j}{h_j} > k$ $(h_j \leq h)$, where d_j is the diameter of the circle inscribed in $\mathcal{T}_j$ and h_j is the largest side of $\mathcal{T}_j$.

The conforming finite element spaces for velocity-temperature-radiation and pressure that we use are Taylor-Hood finite elements P_m/P_{m-1} *i.e.*, polynomial of degree m for the velocity-temperature-radiation and polynomial of degree $m-1$ for the pressure, respectively. An illustration of such finite element is depicted in Figure 2. These elements can be defined as

$$\begin{aligned} V_h &= \left\{ v_h \in C^0(\bar{\Omega}) : \quad v_h\big|_{\mathcal{T}_j} \in S(\mathcal{T}_j), \quad \forall\, \mathcal{T}_j \in \Omega_h \right\}, \\ \mathcal{Q}_h &= \left\{ q_h \in C^0(\bar{\Omega}) : \quad q_h\big|_{\mathcal{T}_j} \in R(\mathcal{T}_j), \quad \forall\, \mathcal{T}_j \in \Omega_h \right\}, \end{aligned}$$

where $C^0(\bar{\Omega})$ denotes the space of continuous and bounded functions in $\bar{\Omega}$, $S(\mathcal{T}_j)$ and $R(\mathcal{T}_j)$ are polynomial spaces defined in $\mathcal{T}_j$ as $S(\mathcal{T}_j) = P_m(\mathcal{T}_j)$ and $R(\mathcal{T}_j) = P_{m-1}(\mathcal{T}_j)$.

Let us choose a time step Δt and discretize the time interval into subintervals $[t_n, t_{n+1}]$ with $t_n = n\Delta t$. For any generic function w we use the notation $w^n(\mathbf{x}) = w(\mathbf{x}, t_n)$. Hence, we formulate the finite element

solutions to $u^n(\mathbf{x})$, $v^n(\mathbf{x})$, $T^n(\mathbf{x})$, $\varphi^n(\mathbf{x})$ and $p^n(\mathbf{x})$ as

$$u_h^n = \sum_{j=1}^{M} U_j^n \phi_j, \qquad v_h^n = \sum_{j=1}^{M} V_j^n \phi_j, \qquad T_h^n = \sum_{j=1}^{M} \Lambda_j^n \phi_j, \qquad \varphi_h^n = \sum_{j=1}^{M} \xi_j^n \phi_j, \qquad p_h^n = \sum_{j=1}^{N} P_j^n \psi_j, \tag{23}$$

where M and N are respectively, the number of velocity-temperature-radiation and pressure mesh points in the partition Ω_h. The functions U_j^n, V_j^n, Λ_j^n, ξ_j^n and P_j^n are respectively, the corresponding nodal values of $u_h^n(\mathbf{x})$, $v_h^n(\mathbf{x})$, $T_h^n(\mathbf{x})$, $\varphi_h^n(\mathbf{x})$ and $p_h^n(\mathbf{x})$ defined as $U_j^n = u_h^n(\mathbf{x}_j)$, $V_j^n = v_h^n(\mathbf{x}_j)$, $\Lambda_j^n = T_h^n(\mathbf{x}_j)$, $\xi_j^n = \varphi_h^n(\mathbf{x}_j)$ and $P_j^n = p_h^n(\mathbf{y}_j)$ where $\{\mathbf{x}_j\}_{j=1}^M$ and $\{\mathbf{y}_j\}_{j=1}^N$ are the set of velocity-temperature-radiation and pressure mesh points in the partition Ω_h, respectively, so that $N < M$ and $\{\mathbf{y}_1, \ldots, \mathbf{y}_N\} \subset \{\mathbf{x}_1, \ldots, \mathbf{x}_M\}$. In (23), $\{\phi_j\}_{j=1}^M$ and $\{\psi_j\}_{j=1}^N$ are respectively, the set of global nodal basis functions of V_h and $\mathcal{Q}_h$ characterized by the property $\phi_i(\mathbf{x}_j) = \delta_{ij}$ and $\psi_i(\mathbf{y}_j) = \delta_{ij}$ with δ_{ij} denoting the Kronecker symbol. In what follows we formulate the two main stages in our Galerkin-characteristic method namely, the Lagrangian stage and the Eulerian stage.

4.1. *Solution Procedure: The Lagrangian Stage*

Let us denote by $\mathbf{X}(\mathbf{x}, t_{n+1}; t)$ the characteristic curves associated with the material derivative (10) which solve the following initial value problem

$$\begin{aligned} \frac{d\mathbf{X}(\mathbf{x}, t_{n+1}; t)}{dt} &= \mathbf{u}\left(\mathbf{X}(\mathbf{x}, t_{n+1}; t), t\right), \quad \forall\ (\mathbf{x}, t) \in \bar{\Omega} \times [t_n, t_{n+1}], \\ \mathbf{X}(\mathbf{x}, t_{n+1}; t_{n+1}) &= \mathbf{x}. \end{aligned} \tag{24}$$

Notice that $\mathbf{X}(\mathbf{x}, t_{n+1}; t) = (X(\mathbf{x}, t_{n+1}; t), Y(\mathbf{x}, t_{n+1}; t))^T$ is the departure point and represents the position at time t of a particle that reaches the point $\mathbf{x} = (x, y)^T$ at time t_{n+1}. Hence, for all $\mathbf{x} \in \bar{\Omega}$ and $t \in [t_n, t_{n+1}]$ the solution of (24) can be expressed as

$$\mathbf{X}(\mathbf{x}, t_{n+1}; t_n) = \mathbf{x} - \int_{t_n}^{t_{n+1}} \mathbf{u}\left(\mathbf{X}(\mathbf{x}, t_{n+1}; t), t\right)\, dt. \tag{25}$$

Accurate estimation of the characteristic curves $\mathbf{X}(\mathbf{x}, t_{n+1}; t_n)$ is crucial to the overall accuracy of the Galerkin-characteristic method. In this paper, we used a method first proposed in [30] in the context of semi-Lagrangian schemes to integrate the weather prediction equations. Details on the formulation and the implementation of this step for characteristics-based methods can be found in references [6, 7, 25, 26] and are not repeated here. Assuming that a suitable approximation is made for (25), then $\mathbf{X}(\mathbf{x}, t_{n+1}; t_n)$ would not lie on a spatial position of gridpoint, so it is required that the scheme to compute $\mathbf{X}(\mathbf{x}, t_{n+1}; t_n)$ be equipped with a search-locate algorithm to find the host element where such point is located. For structured meshes this step can be simple as index checking or *ad hoc* searching. To perform this step we have implemented a search-locate algorithm especially designed in [1] for the semi-Lagrangian method that works for triangles elements in unstructured discretizations.

Hence, we discretize the Stokes/Boussinesq step in time using the second-order Crank-Nicolson method for all terms involving velocity and temperature, whereas a first-order implicit Euler scheme is used for

the pressure variable. This can be formulated as

$$\begin{gathered}\nabla \cdot \mathbf{u}^{n+1} = 0, \\ \frac{\mathbf{u}^{n+1} - \tilde{\mathbf{u}}^n}{\Delta t} + \nabla p^{n+1} - \frac{1}{Re}\nabla^2 \mathbf{u}^{n+1/2} = \left(T^{n+1} - \frac{1}{2}\right)\mathbf{e}, \\ \frac{T^{n+1} - \tilde{T}^n}{\Delta t} - \frac{1}{PrRe}\nabla^2 T^{n+1/2} = \frac{1}{PrRe}\frac{1}{\tau Pl}\Big(B(\tilde{T}^n) - \varphi^{n+1}\Big). \\ \frac{\tau^2}{3\kappa}\nabla^2\varphi^{n+1} + \kappa\varphi^{n+1} = 4\pi\kappa B(T^n),\end{gathered} \tag{26}$$

where $\tilde{\mathbf{u}}^n(\mathbf{x}) = \mathbf{u}\left(\mathbf{X}(\mathbf{x}, t_{n+1}; t_n), t_{n+1}\right)$, $\tilde{T}^n(\mathbf{x}) = T\left(\mathbf{X}(\mathbf{x}, t_{n+1}; t_n), t_{n+1}\right)$ and

$$w^{n+1/2} = \frac{1}{2}\tilde{w}^n + \frac{1}{2}w^{n+1}.$$

Since $\mathbf{X}(\mathbf{x}, t_{n+1}; t)$ would not coincide on a gridpoint, the velocity and temperature fields at the characteristic feet must be obtained by interpolation from known values at the gridpoints of the element where $\mathbf{X}(\mathbf{x}, t_{n+1}; t)$ belongs. Since our objective in this paper is to combine the modified method of characteristics with the finite element spatial discretization, the Lagrangian interpolation is performed in the host element of departure points using the finite element basis functions as

$$\tilde{u}_h^n = \sum_{j=1}^{M} \tilde{U}_j^n \phi_j, \qquad \tilde{v}_h^n = \sum_{j=1}^{M} \tilde{V}_j^n \phi_j, \qquad \tilde{T}_h^n = \sum_{j=1}^{M} \tilde{\Lambda}_j^n \phi_j, \tag{27}$$

where $\tilde{U}_j^n$, $\tilde{V}_j^n$ and $\tilde{\Lambda}_j^n$ are evaluated by finite element interpolation of $u_h^n(\mathbf{x})$, $v_h^n(\mathbf{x})$ and $T_h^n(\mathbf{x})$ at the feet of characteristic curves $\mathbf{X}(\mathbf{x}, t_{n+1}; t)$. This procedure needs less computational work than using a piecewise exact method for projecting the information from the background Eulerian grid onto the Lagrangian grid as in [4, 19]. Convergence and stability analysis of this class of Eulerian-Lagrangian methods have been studied in [3] for convection-diffusion equations and in [5] for incompressible Navier-Stokes equations.

4.2. *Solution Procedure: The Eulerian Stage*

Now we are in a position to complete the implementation of our Galerkin-characteristic method for the radiation-convection problem (26). Here, we consider a projection-type procedure to solve the Stokes/Boussinesq problem, compare [6] for a similar method. Given $\{p^n, u^n, v^n, T^n, \varphi^n\}$, we compute the solution $\left\{p^{n+1}, u^{n+1}, v^{n+1}, T^{n+1}, \varphi^{n+1}\right\}$ as follows:

Step 1. Solve for the radiative energy φ^{n+1}

$$\frac{\tau^2}{3\kappa}\nabla^2\varphi^{n+1} + \kappa\varphi^{n+1} = 4\pi\kappa B(\tilde{T}^n). \tag{28}$$

Step 2. Solve for the temperature T^{n+1}

$$\frac{T^{n+1} - \tilde{T}^n}{\Delta t} - \frac{1}{PrRe}\nabla^2 T^{n+1/2} = \frac{1}{PrRe}\frac{1}{\tau Pl}\Big(B(\tilde{T}^n) - \varphi^{n+1}\Big). \tag{29}$$

Step 3. Solve for the velocity $\bar{\mathbf{u}}^{n+1}$

$$\frac{\bar{\mathbf{u}}^{n+1}-\tilde{\mathbf{u}}^{n}}{\Delta t}+\nabla p^{n}-\frac{1}{Re}\nabla^{2}\bar{\mathbf{u}}^{n+1/2}=\left(T^{n+1}-\frac{1}{2}\right)\mathbf{e}. \tag{30}$$

Step 4. Solve for the pressure $\bar{p}$

$$\nabla^{2}\bar{p}=\frac{1}{\Delta t}\nabla\cdot\bar{\mathbf{u}}^{n+1}. \tag{31}$$

Step 5. Update the velocity $\mathbf{u}^{n+1}$

$$\frac{\mathbf{u}^{n+1}-\bar{\mathbf{u}}^{n+1}}{\Delta t}+\nabla\bar{p}=\mathbf{0}. \tag{32}$$

Step 6. Update the pressure p^{n+1}

$$p^{n+1}=p^{n}+2\bar{p}. \tag{33}$$

Note that the Poisson problem (31) is obtained by taking the divergence of equation (32) and using the fact that $\nabla\cdot\mathbf{u}=0$. In the solution procedure, four linear systems have to be solved at each time step to update the solution $\left\{p^{n+1},u^{n+1},v^{n+1},T^{n+1},\varphi^{n+1}\right\}$ from (28)-(33). To solve these linear systems in our method we have implemented a preconditioned conjugate gradient algorithm. It should be noted that the finite element discretization of the equations (28)-(32) is trivial and is omitted here. It is described in many text books, see for example [12]. In addition, a detailed reconstruction of the mass and stiff matrices in Galerkin-characteristic solution of convection-dominated flows can be found in [21] among others.

5. Results and Discussions

In this section we present numerical results obtained for the radiation-convection flow past a circular cylinder. In all our computations we set $L=20$, $H=9$, $L'=11$, $D=1$, $Pr=0.71$, $Pl=1$ and $u_\infty=1$. The dimensionless temperature $T_C=-0.5$ and $T_H=0.5$. A time step of $\Delta t=0.1$ is used and computational results are illustrated at time $t=100$ for different optical scales τ and Reynolds numbers Re. We perform computations with the triangular finite element P_2/P_1 using the unstructured meshes shown in Figure 3. All the linear systems of algebraic equations are solved using the conjugate gradient solver with incomplete Cholesky decomposition (ICCG) as a preconditioner. Furthermore, all stopping criteria for iterative solvers were set to 10^{-5}. In order to quantify our results we compute the force coefficients

$$\text{lift coefficient}=\frac{F_x}{\frac{1}{2}\rho_\infty u_\infty^2 D}=\oint_0^{2\pi}\mathcal{T}_2\,dx,\qquad \text{drag coefficient}=\frac{F_y}{\frac{1}{2}\rho_\infty u_\infty^2 D}=\oint_0^{2\pi}\mathcal{T}_1\,dx,$$

where $\mathcal{T}=(\mathcal{T}_1,\mathcal{T}_2)^T$ is the traction vector on the cylinder boundary. We also calculate the Strouhal number $St=D/u_\infty\mathbb{T}$ with $\mathbb{T}$ is the time period. This dimensionless number is widely used in experimental studies to quantify the periodic feature in flows past solid bodies.

First we examine the grid convergence in the Galerkin-characteristic method. To this end, we consider four unstructured meshes with different element densities, see Figure 3. Their corresponding statistics are listed in Table 1. In this table we also include the Strouhal number obtained using Mesh A, Mesh B, Mesh C and Mesh D. As can be seen, for the last two mesh levels Mesh C and Mesh D the differences in Strouhal number are very small. To further qualify the results for these meshes we plot in Figure 4 the cross section of the flow variables p, T, u and v obtained for nonradiating (SP_0) model at the mid-height of the channel, $y=H/2$, just behind the cylinder. The results obtained using the coupled convection-radiation SP_1 model are shown in Figure 5. It is easy to see that solutions obtained using the Mesh A are far from

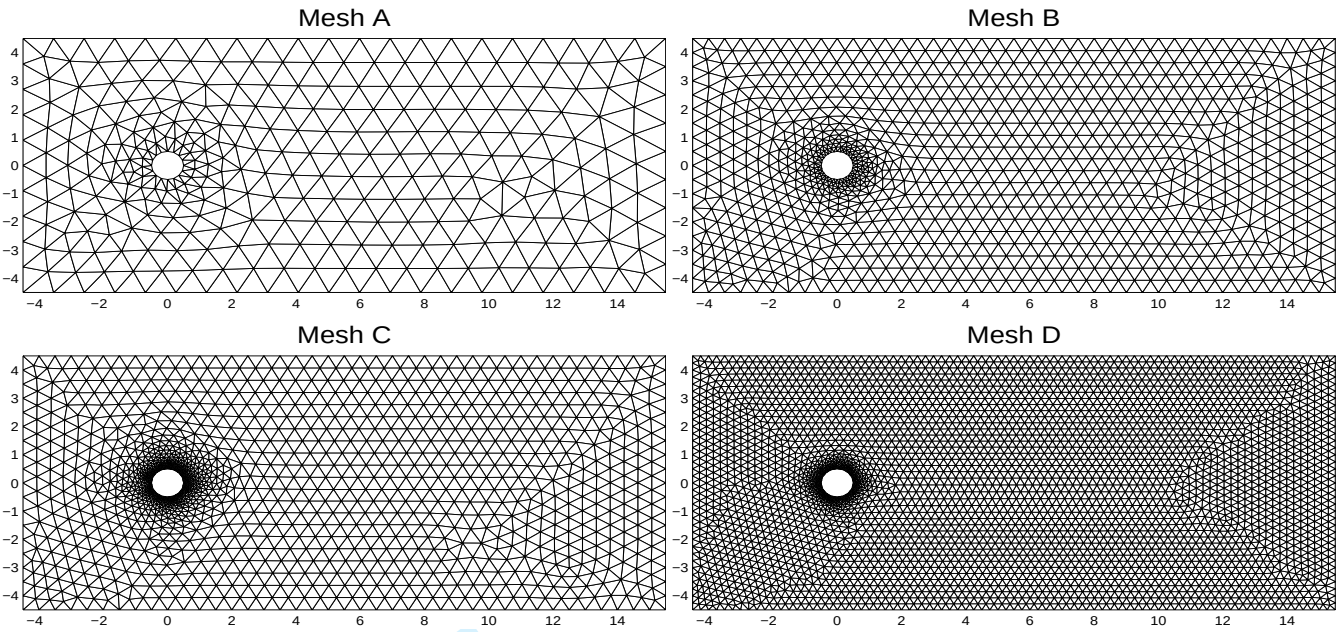

Figure 3. Unstructured meshes used in computations.

Table 1. Mesh statistics and Strouhal numbers for $\tau = 0.5$ and $Re = 100$.

	Number of nodes		Strouhal number	
	$\mathbf{u}$, T and φ	p	SP_0 model	SP_1 model
Mesh A	1227	326	0.1466	0.1311
Mesh B	4188	1084	0.1722	0.1844
Mesh C	5628	1452	0.1750	0.1833
Mesh D	14792	3772	0.1761	0.1834

those obtained by the other meshes. Increasing the density of elements, the results for the Mesh C and Mesh D are roughly similar. Results for other values of optical scales and other Reynolds numbers show the same trends. This ensures grid convergence of the numerical results. Hence, the Mesh C is used in all our next computations. The reasons for choosing this mesh structure lie essentially on the computational cost required for each mesh configuration and also on the numerical resolution obtained.

In order to have a comparison between the nonradiating convection flow (SP_0 model) and the radiating convection flow (SP_1 model) we display in Figure 6 the isotherms obtained using $\tau = 0.5$ and three Reynolds numbers $Re = 60$, $Re = 100$ and $Re = 200$. The velocity fields are presented in Figure 7 for the selected Reynolds numbers. These figures indicate circulation zones moving downstream for both computations with or without including radiation effects. The results also indicate that the inclusion of radiation, by means of the SP_1 model, alters the flow features and also the temperature distribution past the cylinder. For instance, the size of the recirculation zones increase with the flow exhibiting eddies with different magnitudes and separating shear layers. We can see the small complex structures of the flow being captured by the Galerkin-characteristic method.

A numerical comparison between simulations with different optical scales and Reynolds numbers have been also carried out for this problem. The evolution in time of the lift and drag forces for these simulations are displayed in Figure 8. As can be seen, there are little differences in the results obtained without accounting for radiation and those obtained with the SP_1 model with $Re = 60$. These differences become more pronounced in the drag coefficient for the simulation with $Re = 200$.

As a final remark we want to comment on the computational cost for the presented approximations. In Table 2 we summarize the CPU times for the SP_0 and SP_1 models measured on a PC with AMD-K6 200 processor running Fortran codes under Linux 2.2. It is clear that the CPU times required by SP_0 solutions were slightly lower than the respective SP_1 solutions. In all considered Re regimes, the additional work

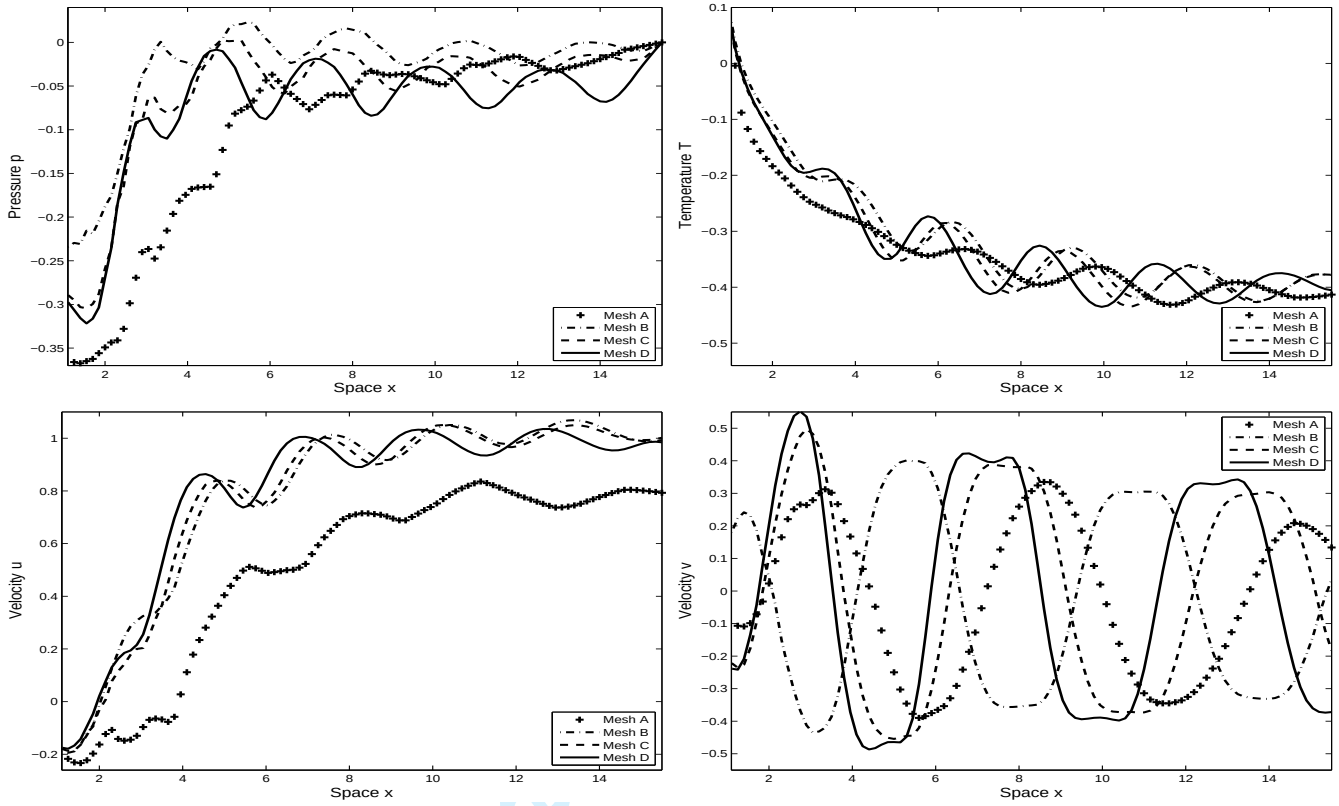

Figure 4. Results for the SP_0 model using four different meshes using $\tau = 0.5$ and $Re = 100$.

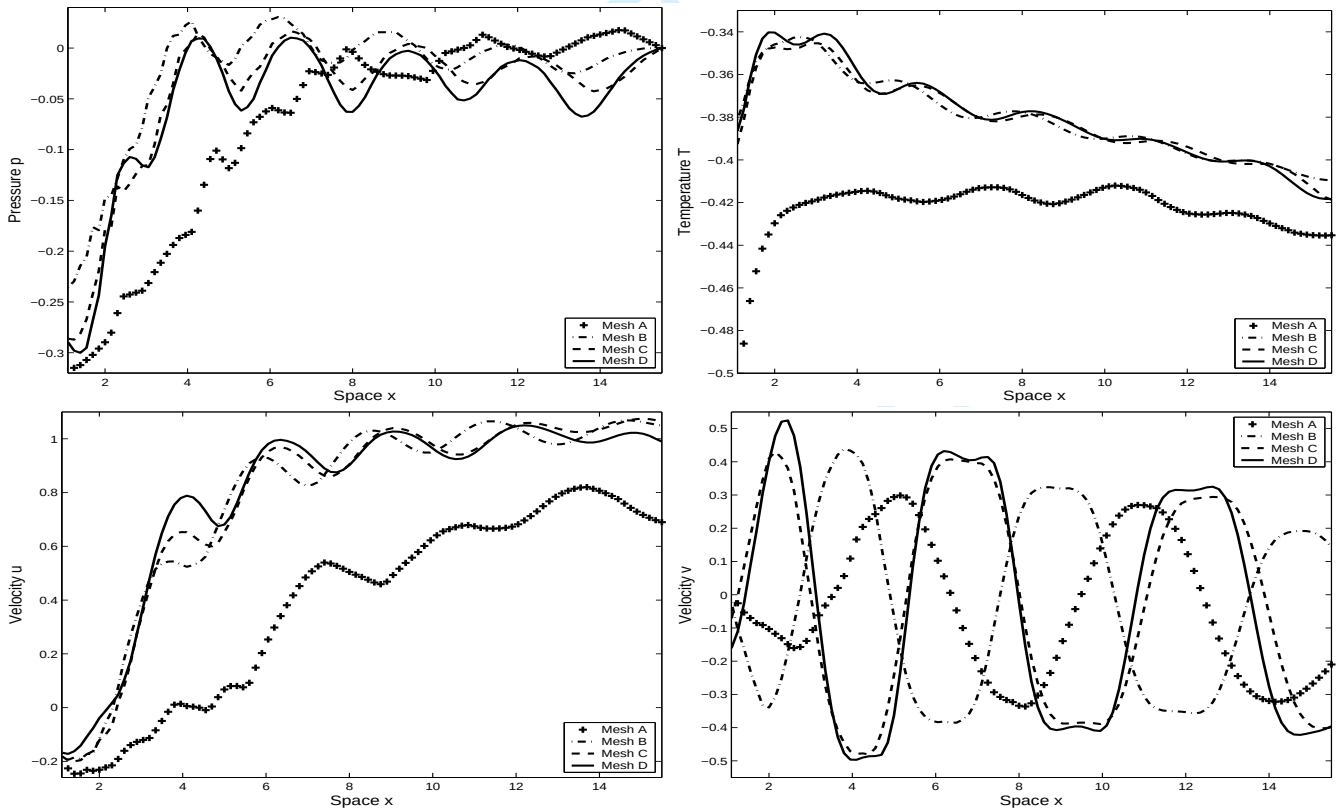

Figure 5. Results for the SP_1 model using four different meshes using $\tau = 0.5$ and $Re = 100$.

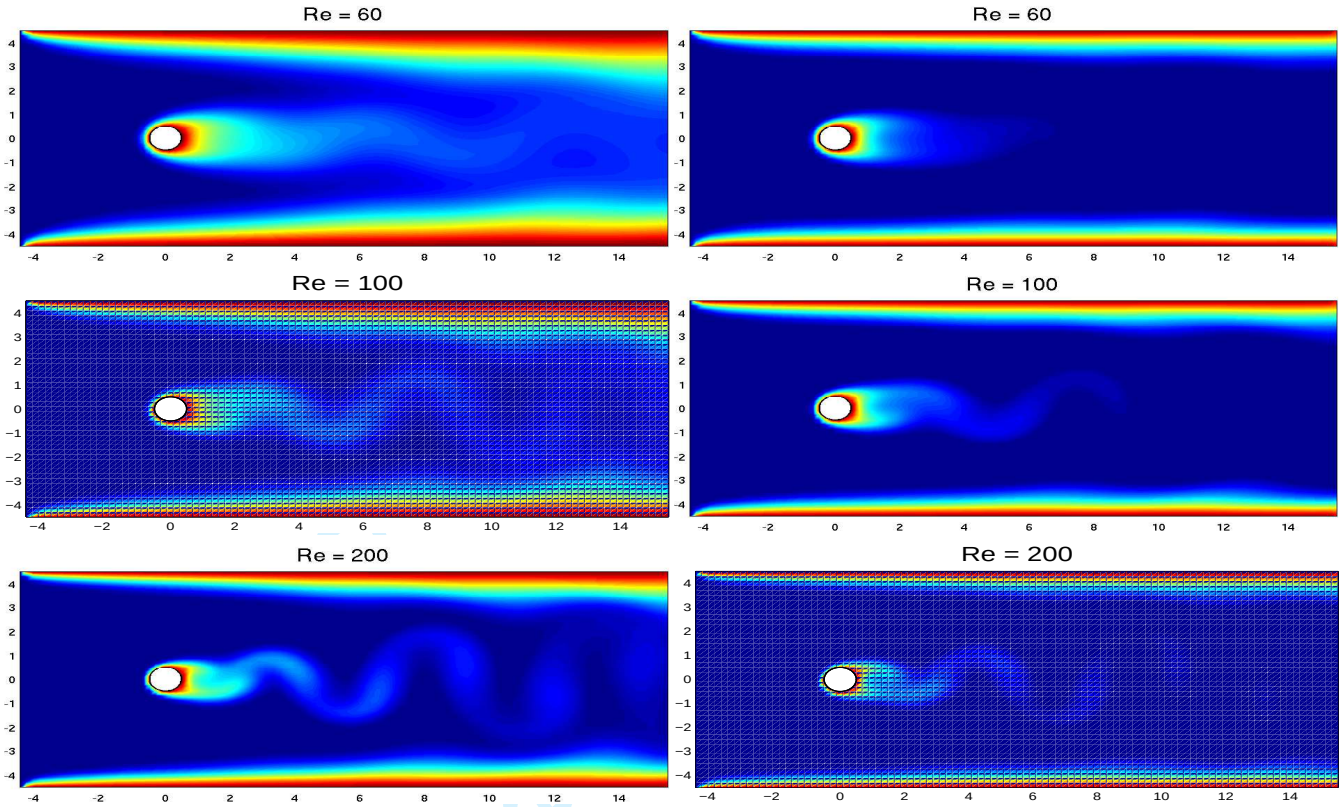

Figure 6. Isotherms for SP_0 model (left column) and SP_1 model (right column) using $\tau = 0.5$.

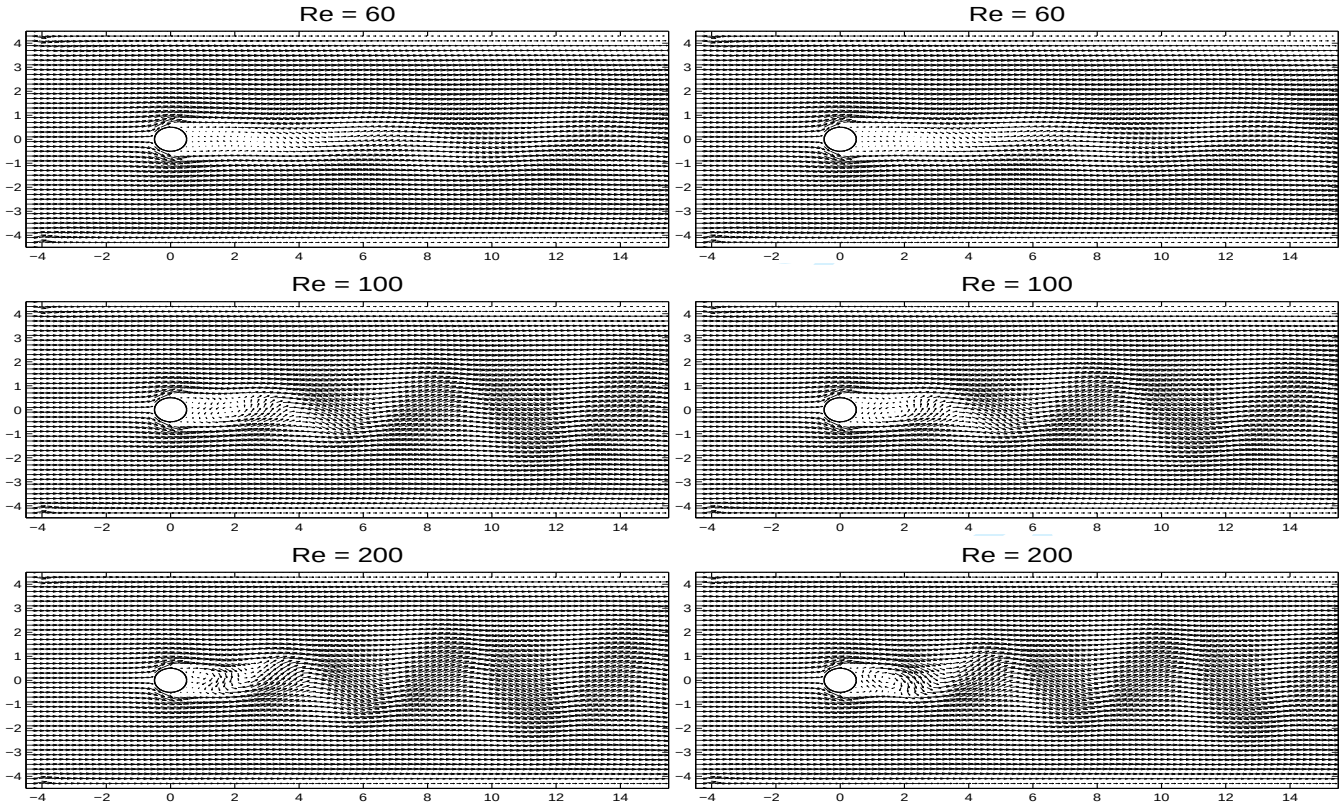

Figure 7. Velocity vectors for SP_0 model (left column) and SP_1 model (right column) using $\tau = 0.5$.

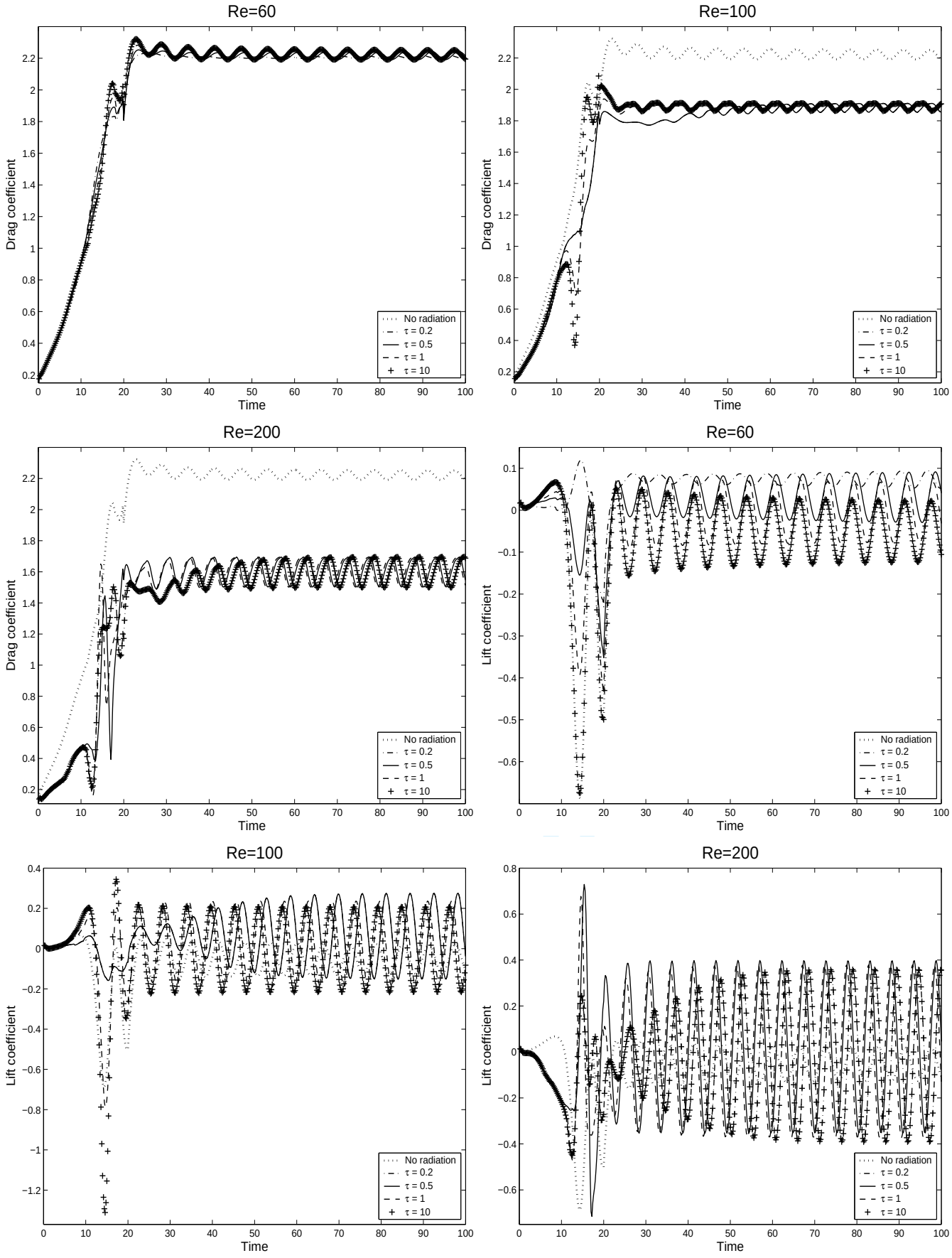

Figure 8. Time evolution of the lift and drag coefficients for $Re = 60$, $Re = 100$ and $Re = 200$.

Table 2. CPU times (in seconds) for the SP_0 and SP_1 models for different Reynolds numbers.

	$\tau = 0.5$			$\tau = 10$		
	$Re = 60$	$Re = 100$	$Re = 200$	$Re = 60$	$Re = 100$	$Re = 200$
without radiation	260	256	249	260	256	249
with SP_1 model	318	307	302	383	380	373

needed to include radiation effects into the thermal flow was less than 60 seconds for $\tau = 0.5$ and 125 seconds for $\tau = 10$.

It is worth remarking that the main part of the computational work in the solution procedure was consumed by the ICCG solver. In our Galerkin-characteristic algorithm, the number of iterations to reach the tolerance of 10^{-5} do not overpass 15 iterations for the velocity/temperature and 40 iterations for the Poisson problems for the pressure and radiative energy at most Re numbers. Needless to say that the algorithm presented in this paper can be highly optimized for the vector computers, because they not require nonlinear solvers and contain no recursive elements. Some difficulties arise from the fact that for efficient vectorization the data should be stored continuously within long vectors rather than two-dimensional arrays.

6. Concluding Remarks

In the present study, the laminar radiation-convection flow past a circular cylinder is numerically solved by a robust Galerkin-characteristic finite element method. The method uses primitive variables in the governing equations and belongs to the class of fractional step procedures where convection part and Stokes/Boussinesq part are treated separately. Second-order accuracy in time is achieved thanks to the Crank-Nicolson differentiation of the total derivative for velocity and temperature fields. The inclusion of radiation is carried out using the simplified P_1 approximation of the radiative transfer equation. The numerical simulations are performed and comparisons are presented for simulations with and without taking into account the radiation effects in thermal flow past a circular cylinder. The presented results demonstrate the capability of the Galerkin-characteristic finite element method that can provide insight to complex radiation-convection flow behaviors.

Future work will concentrate on developing efficient solvers for the associated linear systems and extension of these techniques to higher order simplified P_N approximations.

Acknowledgements. The work by M. El-Amrani has been supported by Deutscher Akademischer Austausch Dienst (DAAD) grant A/06/12950. The work by M. Seaïd has been partially supported by Deutschen ForschungsGemeinschaft (DFG) through the SFB568.

References

[1] A. Allievi, R. Bermejo, 1997, A generalized particle search-locate algorithm for arbitrary grids. *J. Comp. Physics,* **132**, 157–166.
[2] R. Backofen, T. Bilz, A. Ribalta, A. Voigt, 2004 SP_N-Approximations of Internal Radiation in Crystal Growth of Optical Materials. *J. Crystal Growth.,* **266**, 264–270.
[3] R. Bermejo, M. El-Amrani, A Finite Element Semi-Lagrangian Explicit Runge-Kutta-Chebyshev Method for Convection Dominated Reaction-Diffusion Problems. J. Comp. Applied Math., 154:27–61, 2003.
[4] J. Douglas, T.F. Russell, Numerical methods for convection dominated diffusion problems based on combining the method of characteristics with finite elements or finite differences. SIAM J. Numer. Anal. 1982; **19**:871–885.
[5] M. El-Amrani, M. Seaïd, Convergence and stability of finite element modified method of characteristics for the incompressible Navier-Stokes equations. Submitted.
[6] M. El-Amrani, M. Seaïd, Numerical simulation of natural and mixed convection flows by Galerkin-characteristic method. Int. J. Num. Meth. Fluids. (2006) in press.
[7] M. El-Amrani, M. Seaïd, Weakly compressible and advection approximations of incompressible viscous flows. Commun. Numer. Meth. Engng. 2006; **22**:831–847.
[8] M. Frank, M. Seaïd, J. Janicka, A. Klar, R. Pinnau and G. Thömmes, A Comparison of Approximate Models for Radiation in Gas Turbines. Int. J. Progress in CFD. **3** (2004) 191–197.
[9] E.M. Gelbard, Simplified Spherical Harmonics Equations and their Use in Shielding Problems. Technical Report WAPD-T-1182, Bettis Atomic Power Laboratory, 1961.
[10] MR. Graham. The effects of waves on vortex shedding from cylinders. IUTAM Symposium on Buff-Body Wakes, Dynamics and Instabilities, Gottingen, Germany, 1992.

[11] Y. Jaluria, Natural Convection Heat and Mass Transfer. Pergamon Ress, Oxford, 1980.
[12] C. Johnson, Numerical solution of partial differential equations by the finite element method. Cambridge University Press: Cambridge-Lund, 1987.
[13] RN. Kieft, CM. Rindt, AA. van Steenhoven, JF. Van Heijst, On the Wake Structure Behind a Heated Horizontal Cylinder in Cross-Flow. J. Fluid Mech., 486:189–211, 2003.
[14] A. Klar, J. Lang and M. Seaïd, Adaptive Solutions of SP_N-Approximations to Radiative Heat Transfer in Glass. Int. J. Thermal Sciences. 44 (2005) 1013–1023.
[15] E. Larsen, J. Morel and J. McGhee, Asymptotic Derivation of the Multigroup P_1 and Simplified P_N Equations with Anisotropic Scattering. Nucl. Sci. Eng. 123 (1996) 328–367.
[16] E. Larsen, G. Thömmes, A. Klar, M. Seaïd and T. Götz, Simplified P_N Approximations to the Equations of Radiative Heat Transfer and Applications. J. Comp. Phys. 183 (2002) 652–675.
[17] D. Mihalas and B. S. Mihalas, Foundations of Radiation Hydrodynamics. Oxford University Press, New York, 1983.
[18] M. F. Modest, Radiative Heat Transfer. McGraw-Hill, 1993.
[19] O. Pironneau, On the transport-diffusion algorithm and its applications to the Navier-Stokes equations. Numer. Math. 1982; 38:309–332.
[20] M. Schäfer, S. Turek, Benchmark computations of laminar flow around a cylinder. Notes on Numerical Fluid Mechanics 1996; 52:547–566.
[21] M. Seaïd and M. El-Amrani, Lagrange-Galerkin method for unsteady free surface water waves. Computing and Visualization in Science. (2006) in press.
[22] M. Seaïd, Multigrid Newton-Krylov Method for Radiation in Diffusive Semitransparent Media. J. Comp. Applied Math. (2006) in press.
[23] M. Seaïd, A. Klar and R. Pinnau, Numerical Solvers for Radiation and Conduction in High Temperature Gas Flows. J. Flow Turbulence and Combustion. 75 (2005) 173–190.
[24] M. Seaïd, M. Frank, A. Klar, R. Pinnau and G. Thömmes, Efficient Numerical Methods for Radiation in Gas Turbines. J. Comp. Applied Math. 170 (2004) 217–239.
[25] M. Seaïd. Semi-Lagrangian Integration Schemes for Viscous Incompressible Flows. J. Comp. Methods in App. Math., 4:392–409, 2002.
[26] M. Seaïd. On the Quasi-Monotone Modified Method of Characteristics for Transport-Diffusion Problems with Reactive Sources. J. Comp. Methods in App. Math., 2:186–210, 2002.
[27] E. Schneider, M. Seaïd, J. Janicka, A. Klar. Validation of simplified PN models for radiative transfer in combustion systems. Commun. Numer. Meth. Engng., in press, 2006.
[28] J. Simo and F. Armero. Unconditional Stability and Long-term Behavior of Transient Algorithms for the Incompressible Navier-Stokes and Euler Equations. Comp. Methods Appl. Mech. Eng., 111:111–154, 1994.
[29] I. Teleaga, M. Seaïd, I. Gasser, A. Klar, J. Struckmeier, Radiation Models for Thermal Flows at Low Mach Number. J. Comp. Phys. 215 (2006) 506–525.
[30] C. Temperton, A. Staniforth, An Efficient Two-time-level Semi-Lagrangian Semi-implicit Integration Scheme. Quart. J. Roy. Meteor. Soc., 113 (1987) 1025–1039.
[31] G. Thömmes, R. Pinnau, M. Seaïd, T. Götz and A. Klar, Numerical Methods and Optimal Control for Glass Cooling Processes. Transp. Theory Stat. Phys. **31** (2002) 513–529.